Effect of Nb content on hydrothermal stability of a novel ethylene-bridged silsesquioxane molecular sieving membrane for H_2/CO_2 separation

Hong Qi*, Huiru Chen, Li Li, Guizhi Zhu, Nanping Xu

State Key Laboratory of Materials-Oriented Chemical Engineering, Membrane Science and Technology Research Center, Nanjing University of Technology, Nanjing 210009, China

ABSTRACT

Silica-based microporous membranes for the separation of gases with relatively small kinetic diameters, like hydrogen, carbon dioxide, nitrogen and oxygen under harsh industrial processes, will offer great potential for integration in CO_2 capture technologies. Development of membranes with integrated performances of permeability, selectivity and stability in the presence of hot vapor, is one of the prerequisites for their successful implementation. Herein, we reported a novel microporous hybrid silica membrane, fabricated through sol–gel deposition of an ethylene-bridged silsesquioxane layer on a multilayer porous support, by adjusting the amount of niobium alkoxide precursor. When the Nb content was less than 50% (in mole), both hybrid siliceous microporous networks and generated Lewis acid sites imparted very low CO_2 permeance to the membrane while retaining its comparatively high H_2 permeance. Dominant densification shall take effect when Nb content was higher than 50%, which leads to both low H_2 permeance and H_2/CO_2 permselectivity. Hybrid silica membranes with niobium loading amount of 17% and 33% respectively, showed excellent stabilities in the presence of 150 kPa steam under 200 °C, as evidenced by steady H_2 permeances and exceptionally high H_2/CO_2 permselectivities (> 700) during long-term stability test up to 300 h, which demonstrating a promising CO_2 separation membrane.

© 2012 Elsevier B.V. All rights reserved.

1. Introduction

The reduction or elimination of CO_2 emissions from electricity generation power plants fueled by coal or gas, which is approximately account for one third of the main anthropogenic sources of CO_2 [1], will greatly reduce green house gas emissions, which are generally believed to be responsible for global warming. There are three main approaches to CO_2 capture for power plant applications, as post-combustion, oxy-fuel combustion and pre-combustion, which corresponds to the separation of CO_2/N_2, O_2/N_2 and H_2/CO_2, [2]. The disadvantages of existing technologies for the separation of above-mentioned gas mixtures, like cryogenic distillation, solvents absorption and adsorption (PSA), include high energy costs, consumption of sorbents, and complicated processing [3]. Therefore, developing more viable and effective gas separation technology is urgently needed for CO_2 mitigation. As an environmental-friendly alternative to the conventional gas separation technologies, membrane-based separation processes have drawn a great deal of attention in recent two decades, due to its high energy efficiency and simple continuous processes [1]. Inorganic membranes technology for the separation of gases,

especially which with the kinetic diameter smaller than 0.5 nm (e.g. H_2, CO_2, CO, N_2, O_2, CH_4), is foreseen to play an important role in reducing the environmental impact and costs of many industrial processes, owing to their thermal, mechanical, and chemical stability under harsh environments where its polymeric counterpart cannot be applied [4,5]. Inorganic membranes that can separate hydrogen from CO_2-containing gas streams with subsequent CO_2 sequestration, offer great potential for integration in pre-combustion CO_2 capture technologies and, hence, being a rather hot topic in the present membrane research field. Several inorganic materials have been proposed to be used as gas separation membranes for such purpose, including zeolites [6–9], carbon [10–13], silica [14–34] and metal oxides [35,36]. Among these, silica-based microporous membranes with the pore size tailored to the gas molecular range is one of the most promising materials since Uhlhorn et al. [37] firstly found their molecular sieving performances in 1989. Since then, silica-based membranes are by far the most extensively investigated gas separation materials. Although TEOS-derived pure silica membranes displayed both high flux and high selectivity [14], the low stability of this membrane in the presence of steam at a temperature as low as 60 °C [38] prevent from application in industrial processes. Further researches that focused mainly on metal or transition-metal (e.g. Ni, Co, Mg, Al, Zr, Ti, Fe, Nb, Pd.) doped silica membranes [16,17,19,25,27–29,39–44] came into

---

* Corresponding author. Tel.: +86 25 83172279; fax: +86 25 83172292.
  E-mail addresses: hqinjut@yahoo.com.cn, hqi@njut.edu.cn (H. Qi).

scope because highly enhanced hydrothermal stability can be provided. Meanwhile, transition-metal alkoxides were also used as alternative precursors to TEOS for the synthesis of microporous metal oxide membranes, such as TiO_2 and ZrO_2 [35,36]. Unfortunately, the permselectivities of these membranes were only a bit higher than the Knudsen value, which is far from implementation in gas separation. Recently, hydrophobic functional groups modified alkoxysilanes [45,46] as well as bridged silsesquioxanes [47–50] were chosen as precursors to develop microporous hybrid silica membranes, whose hydrophobicity can reduce the interactions between hot vapor and membrane materials and, hence, increasing the hydrothermal stability of these new type of membranes. It can be found in the references cited above, however, that the comparatively high H_2 permeance was often obtained at the expense of the reduction of the H_2/CO_2 selectivity and vice versa, as evidenced in Fig. 1. More important, although sol–gel or CVD derived silica-based membranes exhibited both high permeability and selectivity; the inherently low hydrothermal stability severely restricted their broad implementation in industrial processes, where hot steam is often encountered. Imparting microporous membranes with sufficient high H_2 permeance ($> 5 \times 10^{-6}$ mol m^{-2} s^{-1} pa^{-1}) and H_2/CO_2 selectivity (> 30), while maintaining excellent stability in the presence of hot steam, is one of the prerequisites for their industrial application in Steam Reforming (SR) and/or Water Gas Shift (WGS) reactions, which comprise the pre-combustion capture process. Unfortunately, none of the attempts up to now have succeeded in developing microporous membranes that provided with long-term hydrothermal stability to the degree required for application in SR and WGS reactions. To design and successful fabrication of such membranes that can be used in SR and WGS reactions still remains one of the main challenges for membrane researchers.

The high structural stability of ethylene-bridged silsesquioxane-derived hybrid silica membrane under hydrated conditions can be ascribed to the hydrophobic -Si-CH$_2$-CH$_2$-Si- bridged construction, which was proposed by Castricum et al. [51] and Kanezashi et al. [49]. The niobium doping to the silica membranes should be responsible for the high H_2/CO_2 selectivity, which was reported by Boffa et al. [16,27]. Inspired by observations made by Kanezashi et al. [47] and Boffa et al. [16], we [3] reported a promising sol–gel derived hybrid silica membrane by using ethylene-bridged silsesquioxane and niobium butoxide as

precursors, which exhibited both high enough H_2/CO_2 permselectivity and hydrothermal stability. The H_2/CO_2 permselectivity of such membrane measured at 200 °C varied from an initial value of 220 to a value of ca. 3700 after 311 h of in-situ exposure to 100 kPa stream, while the H_2 permeance retained fairly stable at 4×10^{-8} mol m^{-2} s^{-1} pa^{-1}. Subsequent study [52] indicated that dual effects of densification and surface Lewis acidity render the hybrid membrane high performances, which are of great importance for the separation of CO_2 from CO_2-containing streams.

As a water-tolerant solid acid catalyst [53,54], niobium doping amount into the bridged silsesquioxane derived hybrid siliceous host structures will inevitably affect the membrane performances. Herein, we systematically studied the Nb content on H_2/CO_2 separation properties of the Nb-hybrid silica membranes, especially on long-term stability in the presence of hot steam under a partial pressure as high as 150 kPa.

2. Experimental

2.1. Synthesis of niobium-BTESE derived polymeric sols and fabrication of hybrid silica membranes

Niobium-hybrid silica sols were synthesized by using 1, 2-bis (triethoxysilyl) ethane ((C$_2$H$_5$O)$_3$Si-CH$_2$-CH$_2$-Si(C$_2$H$_5$O)$_3$, BTESE, purity 97%, ABCR) and niobium penta (n)butoxide (NPB, purity 99%, ABCR) as precursors. 5.0 mL BTESE was added to 5.0 mL absolute ethanol (dried, Secco Solv, max. 0.02% H_2O, Merck) in nitrogen glove-box. 0.54 mL nitric acid was drop-wise added into the BTESE solution under vigorous stirring. The mixture was then heated to reflux at 60 °C in a water bath for 90 min. Subsequently, 1.9 mL NPB dissolved in 13.0 mL absolute ethanol, together with another 0.54 mL nitric acid, were drop-wise introduced into above-mentioned sol with the mol ratio of 1: 0.17 (Si:Nb). The refluxing was maintained at 60 °C for an additional 90 min with the final mol ratio of 1:0.17:6.3:0.08:4.45 (BTESE:NPB:ethanol: HNO$_3$: H_2O, henceforth referred to as NS-1 sol). The niobium-BTESE derived polymeric hybrid silica sol was cooled down to the room temperature and diluted for 6 times with ethanol before dip-coating. For the synthesis of NS-2 (with mol ratio of 1:0.33: 6.3:0.08:4.45 for BTESE:NPB:ethanol:HNO$_3$:H_2O), NS-3 (1:0.5:6.3: 0.08:4.45) and NS-4 (1:0.75:6.3:0.08:4.45) sols, similar procedure for the preparation of NS-1 sol was adopted, except that the total adding amount of NPB was 3.75 mL, 5.68 mL and 8.50 mL, respectively. Supported membranes were fabricated through dip-coating afore-mentioned sols onto a home-made disk α-alumina supported mesoporous γ-alumina layer under clean room (class 1000) conditions. After that, niobium-hybrid silica membranes (henceforth denoted as NS-1, NS-2, NS-3 and NS-4 membrane, respectively) were calcined under dry nitrogen atmosphere at 450 °C for 3 h, with the heating and cooling rates of both 0.5 °C min^{-1}. Nb-hybrid silica powders (henceforth designated as NS powders) were obtained by drying corresponding Nb-hybrid silica sols in a Petri dish overnight, followed by calcination procedures which are the same as that found for supported membranes.

2.2. Characterization

Effective particle size in the NS sol was measured by dynamic light scattering (DLS) using a Zetatrac analyzer (Microtrac Inc.). The average hydrodynamic diameters of NS sols reported in this study are the intensity weighted mean diameter derived from a cumulant analysis in the Microtrac software. Thermal evolution of dried sol–gel derived NS powders was measured using a combined thermogravimetry and differential thermal
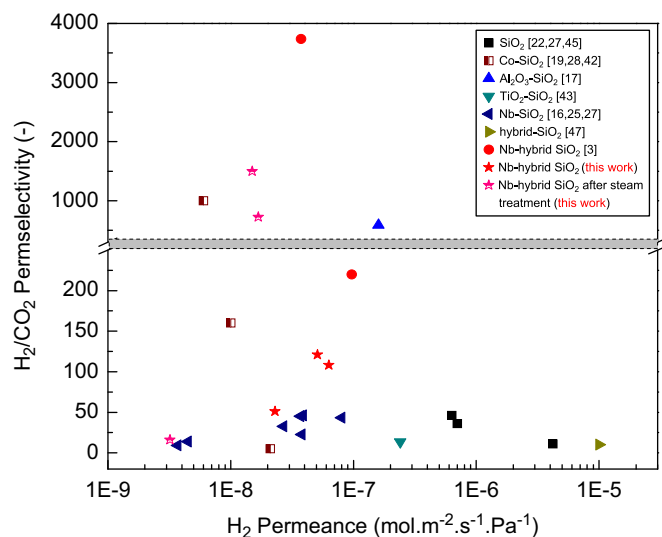

Fig. 1. Comparison of performances of NS membranes (this work) with that of microporous silica and modified silica-based membranes in terms of H_2 permeance and H_2/CO_2 permselectivity.

analysis (TG/DTA) apparatus (STA-449-F3, Netzsch). Measurements were conducted in nitrogen atmosphere (flow rate: 30 mL min^{-1}) with a heating rate of 10 °C min^{-1}. Phase compositions of 450 °C-calcined NS powders as well as powders after steam treatment under a pressure of 1000 kPa, were probed by X-ray diffraction (XRD, Bruker D8, Advance diffractometer), using a target of Cu Kα operated at 40 kV and 40 mA. Fourier transform infrared (FT-IR) spectroscopy was performed both on 450 °C-calcined NS powders and powders after steam treatment in a wave-number region from 4000 to 400 cm^{-1} on a Tensor 27 FT-IR spectrometer (Bruker Optics), using a transmission cell and KBr as reference. Gas adsorption measurements were conducted at 77 K (N$_2$) and 298 K (CO$_2$) on ASAP 2020 (Micromeritics) and Belsorp-mini (Bel Inc.) instruments, respectively. Prior to measurements, all samples were degassed under vacuum at 300 °C for 48 h. Temperature-programmed desorption of ammonia (NH$_3$-TPD, TP5080, Xianquan Co. Ltd. Tianjin, China) technique was used to evaluate the acidity of NS powders before and after steam treatment. 40 mg powders were pre-treated in helium (flow rate: 35.5 mL min^{-1}) at 300 °C for 1 h prior to ammonia adsorption, which was carried out at 100 °C for 1 h. Helium was subsequently introduced once again till the baseline was stabled. After that, the system reached a temperature of 900 °C at a heating rate of 10 °C min^{-1}, under which desorption process occurred. NH$_3$-TPD signals were detected with TCD detector. X-ray photoelectron spectroscopy (XPS) measurements were performed on an ESCA-LAB 250 spectrometer (Thermal Electron) equipped with a monochromatic Al Kα X-ray source (1486.6 eV). Binding energies (BE) of Nb 3d and O 1s were determined by computer fitting the measured spectra and were referenced to the C 1s peak of the adventitious carbon (284.8 eV). The type of acid sites presented in NS membranes was determined by a Perkin-Elmer 2000 FT-IR spectrometry using pyridine as the probe molecule. Dried NS powders were first evacuated (10^{-2} Pa), followed by activation procedure carried out under 400 °C for 1 h, then cooled down to the room temperature. The powders were subsequently exposed to pyridine vapors at room temperature for 1 h, followed by desorption of pyridine at 200 °C for another 1 h. Pyridine adsorption infrared spectra were recorded at room temperature in a wave-number region from 1700 cm^{-1} to 1400 cm^{-1}. Solid state ^{29}Si MAS NMR spectra were used to qualitatively determine the silanol groups presented in BTESE and NS-2 powders, which were recorded using a Bruker Avance 400D spectrometer with a spinning frequency of 5 kHz.

Single gas permeation measurements of NS membranes were conducted in a dead-end mode set-up. The membranes were sealed in a stainless steel module using fluoroelastomer O-rings with the separation layer exposed to the feed side. The pressure differential across the membrane was 0.3 MPa, while the permeate side was vent to the atmosphere. Prior to measurements, all membranes were dried overnight at 200 °C. The gas permeances of niobium-hybrid silica membranes were measured at a temperature of 200 °C in a sequence, starting with the smallest kinetic diameter, from H$_2$ (0.289 nm), CO$_2$ (0.33 nm), O$_2$ (0.346 nm), N$_2$ (0.365 nm), CH$_4$ (0.382 nm) to SF$_6$ (0.55 nm). All gas permeances were measured at 200 °C and 0.3 MPa. Since no difference was observed for the single gas permeances of NS membranes when the different test sequence was carried out, i.e. that a second measurement with H$_2$ immediately after CO$_2$ permeation leads to the same results than before, gas permselectivity of the membrane, also known as an ideal selectivity, was calculated based on ratios between permeance values for pure gas throughout this study. Hydrothermal stability of the membranes was tested by measuring their single gas permeances at 200 °C, before and after in-situ exposure to steam at a pressure of 150 kPa over a total period of 300 h. Further stability tests were carried

out by subjecting NS powders to saturated steam at 180 °C (corresponding to a pressure of 1000 kPa) in an autoclave for 30 h and 300 h, respectively. N$_2$ and CO$_2$ gas adsorption measurements, FT-IR, XRD, XPS as well as NH$_3$-TPD characterizations were conducted on those samples and compared with that of corresponding NS powders without steam treatment, so as to assess the hydrothermal stability of NS powders with the steam exposure time.

3. Results and discussion

3.1. Effect of Nb content on H$_2$/CO$_2$ separation property of hybrid silica membranes

Single gas permeances of BTESE-derived membrane containing various niobium contents as a function of kinetic diameter of permeating gas molecule, measured at 200 °C and 0.3 MPa, are displayed in Fig. 2. As can be seen in Fig. 2, all niobium-hybrid silica membranes exhibited decreased single gas (H$_2$, CO$_2$, O$_2$, N$_2$, CH$_4$ and SF$_6$) permeances as the kinetic diameter of gases (except for CO$_2$) increased, indicating membranes provided with molecular sieving characteristic. No difference was observed for the single gas permeances of NS-1 and NS-2 membranes when the different test sequence was carried out, i.e. that a second measurement with H$_2$ immediately after CO$_2$ permeation leads to the same results than before and, hence, gas permselectivity of the NS membranes, also known as an ideal selectivity, was calculated based on ratios between permeance values for pure gas. NS-1 and NS-2 membranes, containing niobium amount of 17% and 33% respectively, showed similar single gas permeances, as evidenced by the hydrogen permeance and H$_2$/CO$_2$ permselectivity were 6.28 × 10^{-8} mol m^{-2} s^{-1} pa^{-1}, 108 (NS-1 membrane) and 5.1 × 10^{-8} mol m^{-2} s^{-1} pa^{-1}, 121 (NS-2 membrane), respectively. A small decline in gas permeances was observed for NS-3 membrane, which provided a more Nb adding amount of 50%. Much lower gas permeances, with the hydrogen permeance as low as 2.1 × 10^{-9} mol m^{-2} s^{-1} pa^{-1}, was found for NS-4 membrane. It should be noted that CO$_2$ transportation through NS-1∼NS-3 membranes showed an irregular tendency as that found for other gases, which should demonstrate a reduced gas
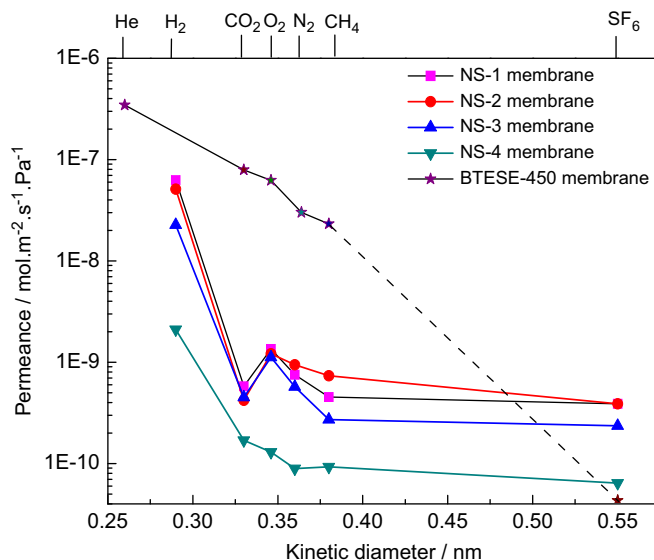

Fig. 2. Single gas permeances of 450 °C-calcined BTESE and NS membranes as a function of the kinetic diameter of the permeating gas molecule measured at 200 °C and 0.3 MPa.

permeance with increasing of kinetic diameter of gases. Additionally, NS membrane showed a decreased H_2/CO_2 permselectivity with the niobium content increased, as displayed in Table S1. It has been reported by Boffa et al. that the increase loading of Nb into silica frameworks led to the densification of materials [16]. The same phenomenon was observed for niobium-hybrid silica membranes in this study, as evidenced by the reduced single gas permeances in comparison with that of pure BTESE-derived hybrid silica membranes. Furthermore, we previously proposed that acid sites arose from the Nb incorporation into hybrid silica membranes may play an important role in obtaining exceptionally low CO_2 permeance.

To clarify the dominant factor in obtaining a high H_2/CO_2 permselectivity of NS membranes, NH_3-TPD test was conducted on Nb_2O_5, BTESE and NS powders, with the results shown in Fig. 3. As can be seen in the upper part of Fig. 3, Nb_2O_5 powder showed an intensive desorption peak at a temperature around 87 °C, indicating the presence of a weak acid site. It is reported [55,56] that NH_3-TPD measurement of TEOS-derived powders displayed a desorption peak below 200 °C, which is the contribution of homogenous Si–O–Si networks and silanol (Si–OH) groups presented in silica membranes. Two peaks were recognized for pure BTESE-derived hybrid silica powders, demonstrating a physical adsorption (at ca. 67 °C) [57,58] and a strong acid site (at ca. 624 °C), which may be the indication of the existence of the Si-CH_2-CH_2-Si frameworks. In comparison with that of Nb_2O_5 and pure BTESE powders, all NH_3-TPD curves of NS powders showed similar profile with two desorption signals occurred at temperature range of 130–197 °C and 550–630 °C, respectively, indicating both a weak and a strong acid site generated. It is worthwhile to note, however, that NH_3-TPD curves of NS powders were not the simple deconvolution of NH_3-TPD data of Nb_2O_5 and pure BTESE powders, as evidenced by the shift of desorption peaks shown in the lower part of Fig. 3. For example, the weak acid site presented

in niobium oxide at ca. 87 °C shifted to higher temperatures of 130 °C, 137 °C, 175 °C and 197 °C in NS powders, respectively. While an opposite variation tendency was apparent for the strong acid site presented in BTESE powder, i.e. the shift of desorption peak at 624 °C to lower temperatures of 618 °C and 547 °C, respectively. It may be the case that niobium was successfully incorporated into hybrid silica networks, with the formation of new microstructures and, hence, altered the acidity of pure BTESE powders.

To verify the presence and type of the acid sites, pyridine adsorption infrared (Py-IR) spectra was carried out on NS-2 powders, with the spectra recorded in the range of 1400–1700 cm^{-1}, are depicted in Fig. 4. As can be seen in Fig. 4, the adsorption peaks occurred at wave numbers of 1415 cm^{-1} and 1463 cm^{-1} can be assigned to Lewis acid sites [59]. The absence of any peaks at around 1540 cm^{-1} demonstrated that either no Brönsted acid site or very few Brönsted acid sites presented in NS powders which cannot be detected by Py-IR instrument [60]. Burke and Ko [61] also found that Nb_2O_5-SiO_2 mixed oxide prepared through co-precipitation showed Lewis acidity, which diminished with the Nb content increased. The results also corroborated our previous hypothesis [52], that it was Lewis acid site rather than Brönsted acid site presented in Nb-BTESE membranes and, hence, affected the CO_2 transportation through microporous hybrid silica membranes.

XRD was employed to determine the status of Nb presented in the Nb-BTESE membranes, with the patterns shown in Fig. S1. Unfortunately, the absence of any Bragg reflections in NS powders indicated the formation of amorphous phases. It may be the case that the niobium composites are either well dispersed on hybrid silica frameworks, or have crystallite sizes smaller than the detection limit for Cu-Kα radiation, as proposed by Francisco and Gushikem [62], and Pereira [63].

It is worthwhile to note that the peak height and area of NH_3-TPD curves of NS-3 and NS-4 powders shown in Fig. 3 were remarkably diminished as compared with that of NS-1 and NS-2, indicating that the acid strength and/or acid sites (density) may greatly reduced with the Nb content [55]. It cannot be excluded, however, that the densification took place in the materials resulted in much lower specific surface area and ensuing narrowed pore size and, hence, prevented ammonia from entering into the membrane pores for adsorption, thus leading to much lower NH_3 desorption
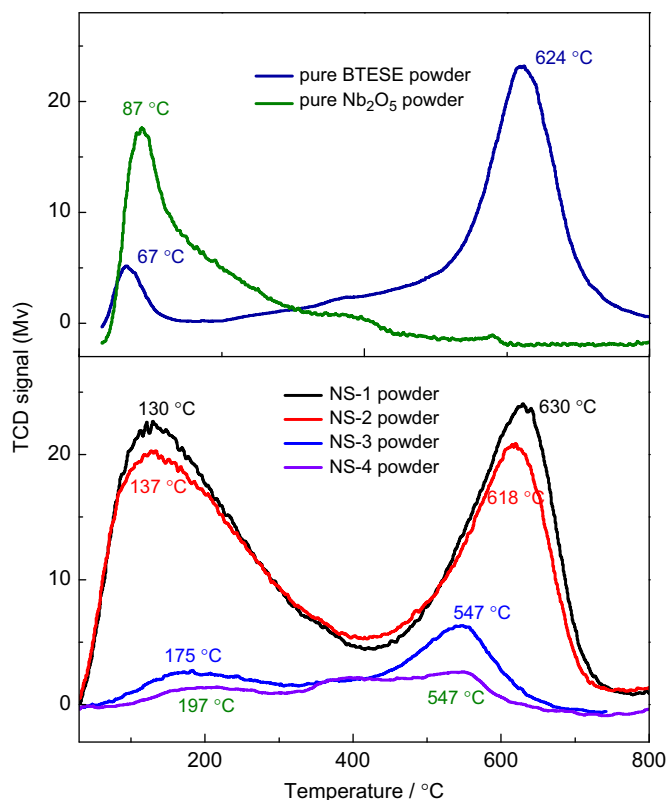

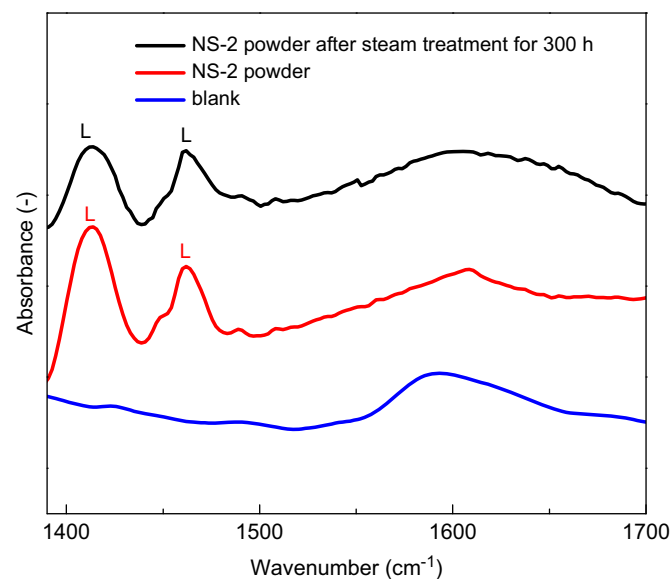Fig. 3. NH_3-TPD curves of hybrid SiO_2(BTESE), Nb_2O_5 and NS powders.

Fig. 4. Py-IR spectra of NS-2 powder before and after steam treatment (1000 kPa for 300 h) that measured at 200 °C.

peaks [55,64]. We [3] and Castricum et al. [38] have previously found that nitrogen gas adsorption at 77 K cannot be observed for NS and BTESE powders, which can be interpreted by the kinetic restrictions either at low temperatures or the relative large kinetic diameter of nitrogen (0.364 nm), as also proposed by Rios et al. [65]. In this study, the same results were found for NS-1∼NS-4 powders. Taking into account that CO_2 has relatively small kinetic diameter of 0.33 nm, CO_2 adsorption isothermals of 450 °C-calcined NS powders with different Nb content, were measured at 298 K and the data, as compared with that of 450 °C-calcined BTESE powders, are given in Fig. 5. As can be seen in Fig. 5, CO_2 adsorption capacities of NS powders decreased with the Nb content, implying that either the acidic strength of powders may increased or more densified material structure was achieved with the niobium adding amount. To clarify the effect of Nb adding amount on NS membrane structures, effective surface areas of NS powders were calculated with the Dubinin method [51] based on the CO_2 adsorption isotherm data shown in Fig. 5, as represented with Eq. (1).

$$\log n = \log n_m + D(\log p^0/p)^2 \tag{1}$$

Subsequently, effective surface areas A can be calculated according to Eq. (2).

$$A = n_m a_m N_A \tag{2}$$

where n is the gas adsorbed at relative pressure p^0/p. n_m is the monolayer adsorption capacity of the surface (mol/g adsorbent). D is an adsorbate-dependent constant. N_A is Avogadro's number and a_m is the area occupied by a molecule in the completed monolayer. Based on Eq. (1), $\log n$ is directly proportional to $(\log p^0/p)^2$. Effective surface area as well as parameter D, $\log n_m$ can be calculated by Eqs. (1) and (2), with the results are displayed in Table S2. As shown in Table S2, effective surface area of NS powders reduced with the niobium adding amount, from 85.6 $m^2 g^{-1}$ (NS-1) to 10.1 $m^2 g^{-1}$ (NS-4). It should be noted, however, that the reduction of effective surface area was not proportional to the increment of niobium content. If we study the niobium addition dependence of the CO_2 adsorption capacities of NS powders, together with NH_3-TPD data displayed in Fig. 3, we can draw a conclusion that the densification was the dominant factor in determining the microstructure of NS powders (or NS membranes). Otherwise, CO_2 adsorption capacities of NS powders should increase with niobium adding amount. NH_3-TPD curves of
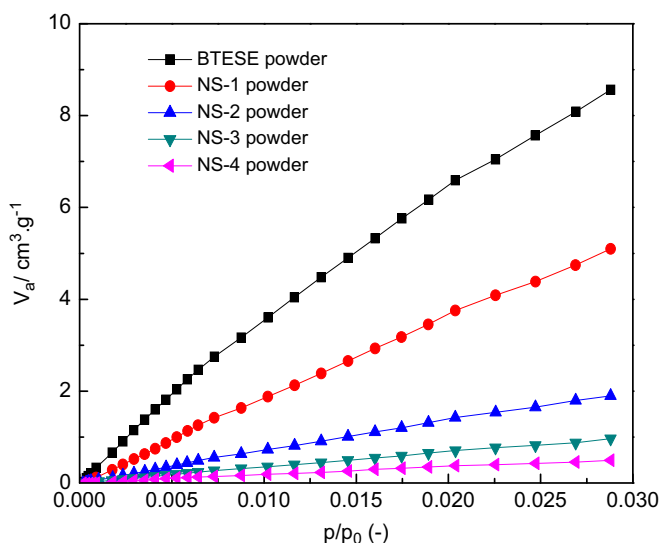

Fig. 5. CO_2 adsorption isotherms (at 298 K) for the calcined BTESE and NS powders.
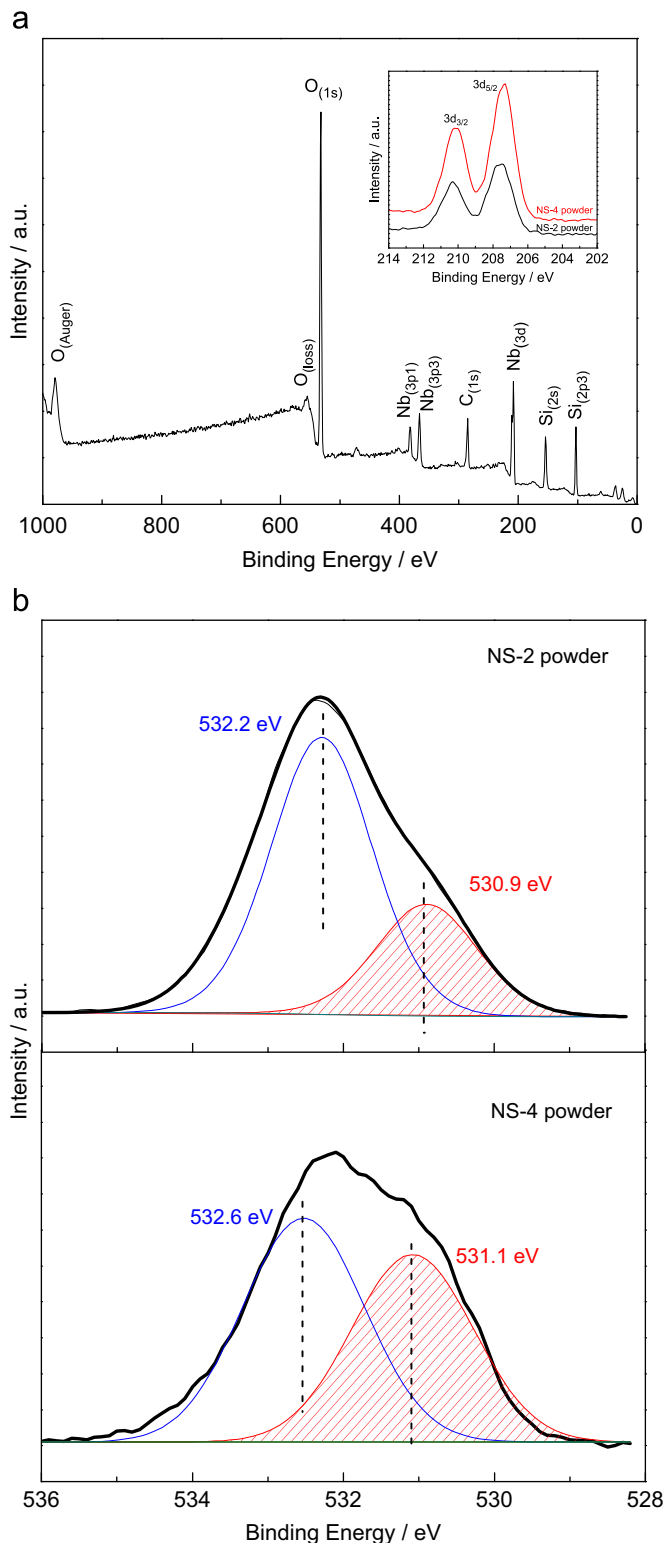

Fig. 6. (a) XPS spectrum of NS powder. Also shown inset is the spectrum of the Nb $3d_{5/2}$ and Nb $3d_{3/2}$ regions for NS-2 and NS-4 powders. (b) XPS spectrum of the O 1s region for NS-2 and NS-4 powders, which is fitted with a Gaussian distribution.

NS powders, on the other hand, are another evidence to identify densified material structures, taken into account the relative smaller kinetic diameter (0.26 nm) of ammonia.

Fourier transform infrared (FT-IR) spectroscopy was employed to monitor the incorporation of Nb into the ethylene-bridged polysilsesquioxane networks, with the FT-IR spectra of

BTESE powders containing various Nb contents are displayed in Fig. S2. All NS powders, together with pure BTESE powder, showed similar spectra regardless of Nb adding amount. The broad vibration at 3500–3000 cm^{-1} should be assigned to stretching of the OH bonds for both H_2O and silanol groups. The band at 1600 cm^{-1} should be assigned to H–O–H bending vibrations. Strong absorption bands appeared in the region of 1000–1100 cm^{-1} as well as the peaks occurred at around 450 cm^{-1}, were caused by Si–O–Si siloxane bridges [66]. The peaks at 2920 cm^{-1} and 1420 cm^{-1} which are slightly visible, were related to the stretching of C–H bonding [38,67] and CH_2 vibrations [68]. Although all NS powders, together with pure BTESE powder, showed similar spectra regardless of niobium content, difference still can be observed in IR spectra of NS powders in comparison with that of BTESE powder in the range of 700–1000 cm^{-1}. As can be seen in Fig. S2, the characteristic symmetric stretching peak of Si–O–Si band at 780 cm^{-1} [69,70] (for pure BTESE powder) is displaced to 901 cm^{-1} (for NS powders). This may be ascribed to the fact that niobium incorporation leads to the formation of Si–O–Nb bondages at silica–niobia interface and, hence, disturbs the vibration of Si–O–Si groups [66]. On the other hand, several authors [71,72] reported that IR bands in the region of 700–900 cm^{-1} is due to Nb–O–Nb modes in bridged niobia compounds, or the Nb–O vibration would produce the asymmetric widening of bands in this region [72]. Therefore, the absence of Nb–O–Nb band in NS powders (this study) is probably due to a very weak and wide intensity, and on the other hand, may be ascribed to the overlapping with the Si–O–Si band at 901 cm^{-1}.

To further probe the micro-structure of niobium-hybrid silica materials, XPS was used to analyze the membrane surface composition as well as the interactions of niobium with the hybrid silica frameworks. The XPS spectra, showing the energy adsorption from Si, C, Nb and O elements, are displayed in Fig. 6(a). Also shown the inset of Fig. 6(a) are the Nb(3d) XPS spectra of NS-2 and NS-4 powders, which suggested that both samples produced a single symmetric 3d$_{5/2}$ component which, on the basis of its binding energy (207.8 ± 0.2 eV), can be assigned to Nb(V) [73,69]. Table 1 shows the elemental composition analysis of NS-2 and NS-4 powders by XPS characterization. The quantitatively elemental composition of NS powders, on the other hand, ensured that successful loading of Nb into the hybrid silica microstructures, and further indicated that the amount of Nb presented in NS powders enhanced as Nb alkoxide precursor addition increased. Fig. 6(b) shows the resulting O 1s photoelectron peak of NS-2 and NS-4 powders. It can be seen that the O 1s peaks for both powders were asymmetrical and can be decoupled into two peaks (530.9 eV (531.1 eV) and 532.2 eV (532.6 eV)) corresponding to O–Nb and Si–O bonds, respectively), which demonstrated the presence of Nb–O–Si, Nb–O–Nb bridges and Si–O–Si siloxane bridges [63,74]. If we compare the O 1s spectrum of NS-2 and NS-4 powders shown in Fig. 6(b), we can observe the slightly shift

of the simulated peak at 530.9 eV and 532.2 eV. Additionally, the intensity of the peak at 530.9 eV strengthened as the Nb adding amount increased. While a reverse tendency was apparent for the peak at 532.2 eV. It can be concluded [55,73,74] that the proportion of Nb–O bridge amounts increased, while O–Si siloxane bridge amounts decreased with the niobium loading based on the calculated area under the corresponding peak and increased FWHM (Full width at half maximum) of O 1s peak, as also evidenced by the XPS results shown in Table 1. To make sure that more Nb–O–Si and/or Nb–O–Nb bridges are formed as Nb incorporated into BTESE powders, solid state ^{29}Si MAS NMR spectrum was used to qualitatively determine the silanol groups presented in BTESE and NS-2 powders, which on one hand could determine the degree of polymerization by using BTESE and NPB as precursors. ^{29}Si MAS NMR is capable of discriminating by characteristic chemical shifts between the five different SiO$_4$ tetrahedra connected with 0–4 other such tetrahedra, i.e. Q^0, Q^1, Q^2, Q^3, and Q^4 (the superscript gives the number, m, of Si–O–Si siloxane bridges of the Si(OSi)$_m$(O-)$_{4-m}$ structural units). The usual values for the mean chemical shifts used to fit the spectra of glasses are −107 ppm (Q^4), −92 ppm (Q^3), −82 ppm (Q^2), −69 ppm (Q^1), and −63 ppm (Q^0), as reported by Du et al. [75]. Solid state ^{29}Si MAS NMR spectra of BTESE and NS-2 powders are shown in Fig. 7. It can be observed in Fig. 7 that the intensity of Q^0 and Q^1 for NS-2 powder was obviously lower than that of BTESE powder. Although the samples were different from Na$_2$O–B$_2$O$_3$–SiO$_2$ glass that was studied by Du et al. [75]. The Q^m distribution
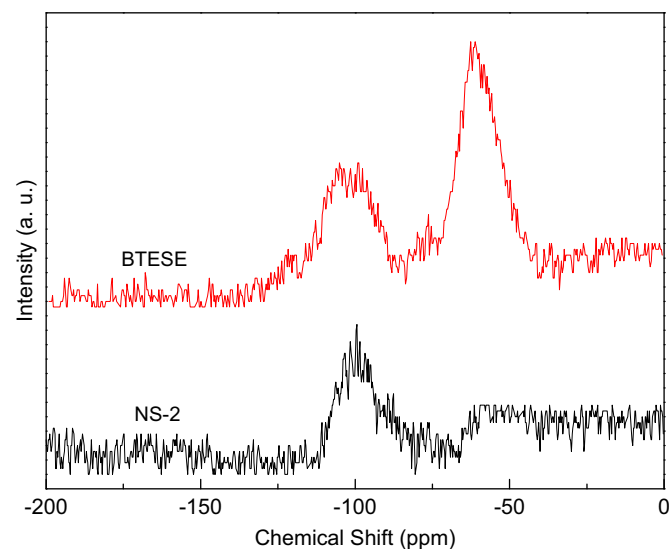

Fig. 7. ^{29}Si MAS NMR spectra of the BTESE and NS-2 powders.

Table 1
Binding energies (BE, eV), full width at half maximum (FWHM, eV) and Nb/Si atomic ratios for NS powders as determined by XPS.

Sample	O 1s peak		Nb 3d$_{5/2}$ peak		Nb/Si atomic ratio
	BE	FWHM	BE	FWHM	
NS-2 powder	532.2 (0.71)[a]	1.65	207.5	1.43	0.27
	530.9 (0.29)[b]	1.65	–	–	–
NS-4 powder	532.6 (0.55)[a]	1.89	207.3	1.52	0.56
	531.1 (0.45)[b]	1.89	–	–	–

[a] Peak area percent of O 1s at ca. 532.2 eV.
[b] Peak area percent of O 1s at ca. 530.9 eV.

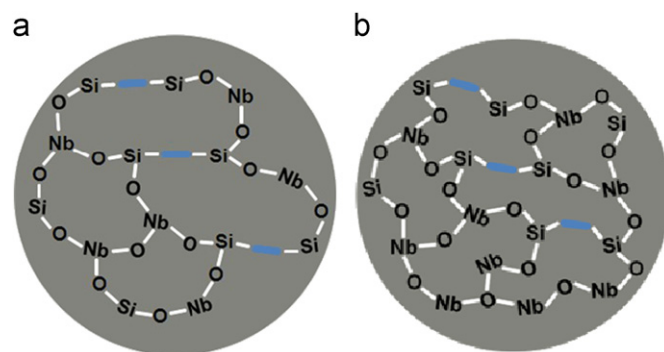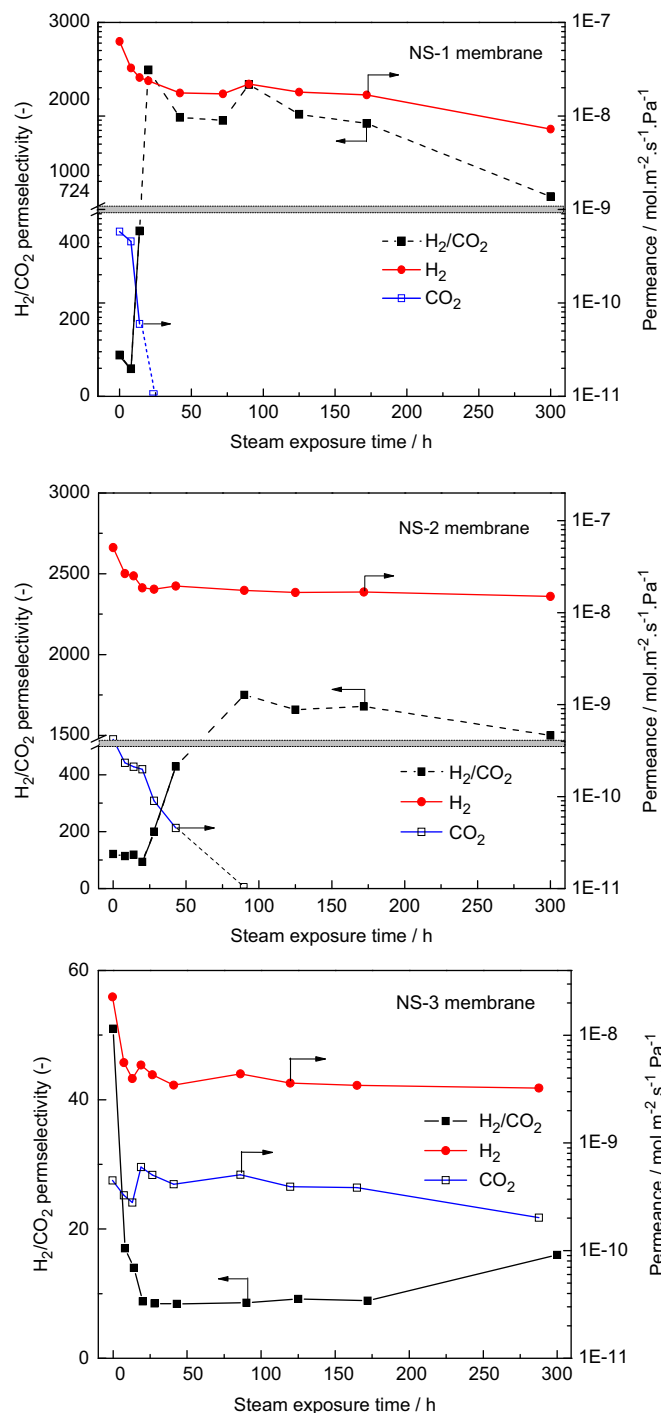**Fig. 8.** Schematic representation of Nb-hybrid SiO$_2$ networks (a) Nb-hybrid SiO$_2$ with low Nb content, (b) Nb-hybrid SiO$_2$ with relatively high Nb content.

Fig. 9. Hydrothermal stability test of NS-1, NS-2 and NS-3 membranes. (Shown are the H_2 and CO_2 gas permeances at 200 °C and the calculated single gas H_2/CO_2 selectivity as a function of the time of exposure to 150 kPa steam).

still can reflect the hydroxyl content, as reported by Drake et al. [76]. Therefore, it can be qualitatively inferred that a greater degree of polymerization occurred in NS-2 powder, as evidenced by the amount of hydroxyl groups presented in NS-2 powder was obviously lower than that of BTESE. The results can further interpret the NH_3-TPD curves of NS powders shown in Fig. 3, i.e. the shift of desorption peaks should be assigned to the formation of Si–O–Nb bridges, inducing a moderate acid site. It is reported that Si–O–Nb shows moderate or strong Lewis acidity [55], which is between the acidity of Nb–O–Nb and Si–C–C–Si bonds. On the other hand, the increasing Nb content leads to the condensation of Nb-OH and Si-OH groups, producing self-condensation (Nb–O–Nb bridges) or cross-condensation (Nb–O–Si bridges) and, hence, results in more densified structures (i.e. densification of NS powders and NS membranes) as was schematically represented in Fig. 8.

3.2. Hydrothermal stability of niobium-hybrid silica membranes

It is well known that silica-based microporous membranes suffer from a serious defect of modest stability under humid conditions [27–29], where industrial processes are often encountered. We [3] have reported that an Nb-hybrid silica membrane exhibited excellent hydrothermal stability over 300 h in the presence of 100 kPa steam. In the above-mentioned sections, we have found that BTESE-derived membranes containing various niobium contents retained relative high H_2 permeance (4×10^{-8} mol m^{-2} s^{-1} pa^{-1}) as well as sufficient high H_2/CO_2 permselectivity (> 50). In this part, the hydrothermal stability of this kind of promising membrane, i.e. BTESE-derived hybrid silica membrane with various niobium amounts, like NS-1, NS-2 and NS-3 membranes, was investigated in detail. The hydrothermal stability of NS membranes was tested by in situ exposure to the 150 kPa steam. Fig. 9 shows H_2 and CO_2 gas permeances at 200 °C and the calculated H_2/CO_2 permselectivity as a function of the time of exposure to 150 kPa steam. With respect to NS-1 and NS-2 membranes, it can be seen that after a small decline during an initial ca. 30 h exposure to steam, the H_2 permeance of both membranes remained fairly constant at a value of $\sim 2 \times 10^{-8}$ mol m^{-2} s^{-1} pa^{-1}, over the entire duration of the steam exposure test. Meanwhile, the CO_2 permeance remained low, decreasing with steam exposure time to reach ultimately a value below the detection limit (ca. 1×10^{-11} mol m^{-2} s^{-1} pa^{-1}). Thus, the H_2/CO_2 selectivity of those two membranes at 200 °C was found to increase during steam treatment, from initial values of 108, 121 to values of ca. 720, 1500, respectively, after 300 h of in-situ exposure to 150 kPa steam. The H_2 permeance of NS-3 membrane varied similar to that found for NS-1 and NS-2 membranes, that is, decreased in the first 30 h and then reached a constant value. Much to our surprise, the CO_2 permeance of NS-3 membrane, although as low as $2–3 \times 10^{-10}$ mol m^{-2} s^{-1} pa^{-1}, was fairly constant during the 300 h steam treatment process. The CO_2 permeance decreased with steam exposure time and reached ultimately a value below the detection limit, as observed in NS-1

Table 2
H_2 and CO_2 permeances of NS-2 membrane before and after steam treatment for 30 h.

Gas	ΔP (MPa)	NS-2 membrane ($\times 10^{-8}$ mol m^{-2} s^{-1} pa^{-1})					NS-2 membrane after steam treatment for 30 h ($\times 10^{-8}$ mol m^{-2} s^{-1} pa^{-1})				
		60 °C	100 °C	125 °C	150 °C	200 °C	60 °C	100 °C	125 °C	150 °C	200 °C
H_2	0.3	0.42	1.1	2.6	3.2	6.9	0.63	1.1	1.4	1.5	3.1
CO_2	0.3	0.012	0.02	0.023	0.037	0.06	0.042	0.055	0.054	0.033	0.015

and NS-2 membranes, was not found for NS-3 membrane. Therefore, the H_2/CO_2 selectivity varied from an initial value of 50 to a value of ca. 10, after 300 h of in situ exposure to 150 kPa steam. Nevertheless, those results showed a promising new type sol–gel derived microporous membrane with sufficient high H_2/CO_2 separation property and excellent hydrothermal stability that may hold great promises in membrane reactor application.

Single gas permeances (H_2 and CO_2) of NS-2 membrane as a function of temperature, before and after steam treatment, are shown in Table 2. The permeances of H_2 and CO_2 across the NS-2 membrane versus temperature are shown in Fig. 10, from which the apparent activation energy (E_a) can be obtained based on the modified Fick law (Eq. (3)) [25], with the calculated E_a displayed in Table 3.

$$P = P_0 \exp\left(-\frac{E_a}{RT}\right) \qquad (3)$$

where P is the membrane permeance, E_a is the apparent activation energy, P_0 is a temperature independent coefficient.

As can be seen in Table 3, the apparent activation energy of permeance in the NS-2 membrane (after steam treatment for 30 h) were 14 kJ mol^{-1} for H_2 and -9.3 kJ mol^{-1} for CO_2, which are all lower than that of corresponding E_a (26.5 kJ mol^{-1} for H_2 and 15.1 kJ mol^{-1} for CO_2) of permeance in the freshly prepared NS-2 membrane. Since E_a in Eq. (3) is the sum of two contributions of E_m (activation energy of mobility) and Q_{st} (isosteric heat of adsorption) with opposite signs, the apparent activation energy can be positive or negative depending on their relative magnitudes [25]. The smaller E_a of H_2 permeance in NS-2 membrane may be explained by either a smaller E_m or a higher Q_{st} or both [77]. A larger E_m is possible when taking into account that much denser structure of NS-2 membrane was obtained after steam

treatment. However, Q_{st} is expected to be much larger after the NS-2 membrane was steam treated, which leads to the lower, or even negative E_a values. The apparent activation energy of permeance in the NS-4 membrane displayed in Table 3 shows similar variation tendency, which also exhibited denser membrane structures in comparison with NS-2 membrane. Nevertheless, more sorption studies of NS membrane materials under relative conditions are expected to lead to a better quantitative understanding of the interaction between Nb and hybrid silica networks.

To shed light on the hydrothermal stability mechanism of this promising Nb-BTESE membrane, the corresponding NS powders that steam-treated in an autoclave for different time intervals were used to probe the alternation of membrane micro-structures. Fig. 11 shows CO_2 isothermal adsorption data of NS-1～NS-3 powders before and after steam exposure. As can be seen in Fig. 11,
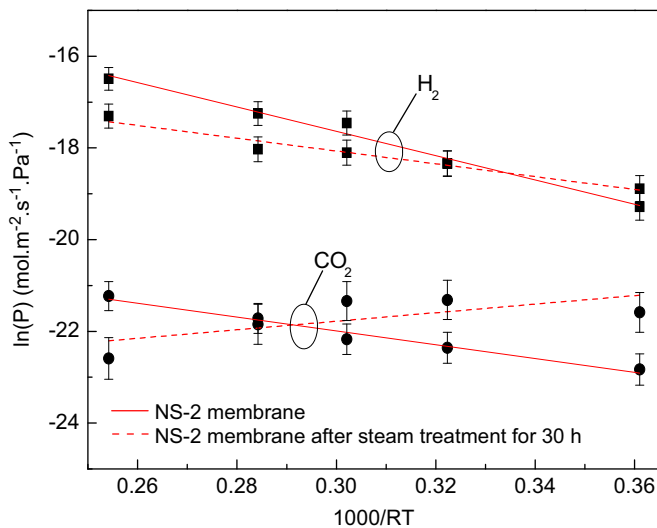

Fig. 10. Arrhenius plot of the H_2 and CO_2 permeance through NS-2 membrane before and after steam treatment for 30 h.

Table 3
Apparent activation energies (E_a) for NS membranes before and after steam treatment for 30 h.

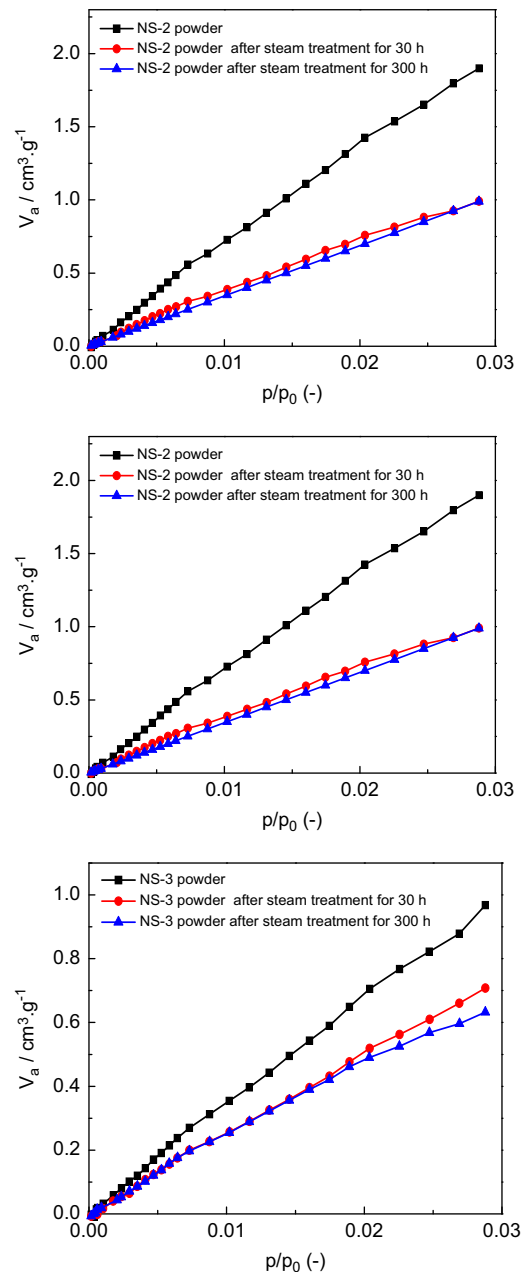| Gas	E_a (kJ/mol) NS-2 membrane	E_a (kJ/mol) NS-2 membrane after steam treatment	E_a (kJ/mol) NS-4 membrane
H_2	26.5	14	14.8
CO_2	15.1	−9.3	−9.7

Fig. 11. CO_2 adsorption isotherms (at 298 K) for the 450 °C-calcined NS powders before and after hydrothermal treatment (powders were hydrothermally-treated in an autoclave at 180 °C for 300 h).

despite of the niobium adding amount, CO_2 sorption capacities of all NS powders were greatly reduced after steam treatment, indicating that either densification took place, or the acidic strength of powders surface increased, as discussed above. With respect to the NS powders steam-treated for different time intervals, little variation of CO_2 adsorption quantity was noticed, indicating that the membrane structures did not alter much as steam exposure time extended. If we study the NH_3-TPD curves shown in Fig. 12, it may be the case that the densification process played a dominant role as the NS powders exposed to the hot steam. As can be seen in Fig. 12, the intensities of desorption peaks for NS powders diminished dramatically with the exposure time to steam. However, it should be noted that NS-1 powders retained acidic characteristic peaks after steam treatment. While NS-2 and NS-3 powders showed fairly weak acidity since almost no desorption peak can be discriminated in Fig. 12. If we analyze the H_2 and CO_2 permeances of NS-1 and NS-2 membranes, CO_2 sorption data
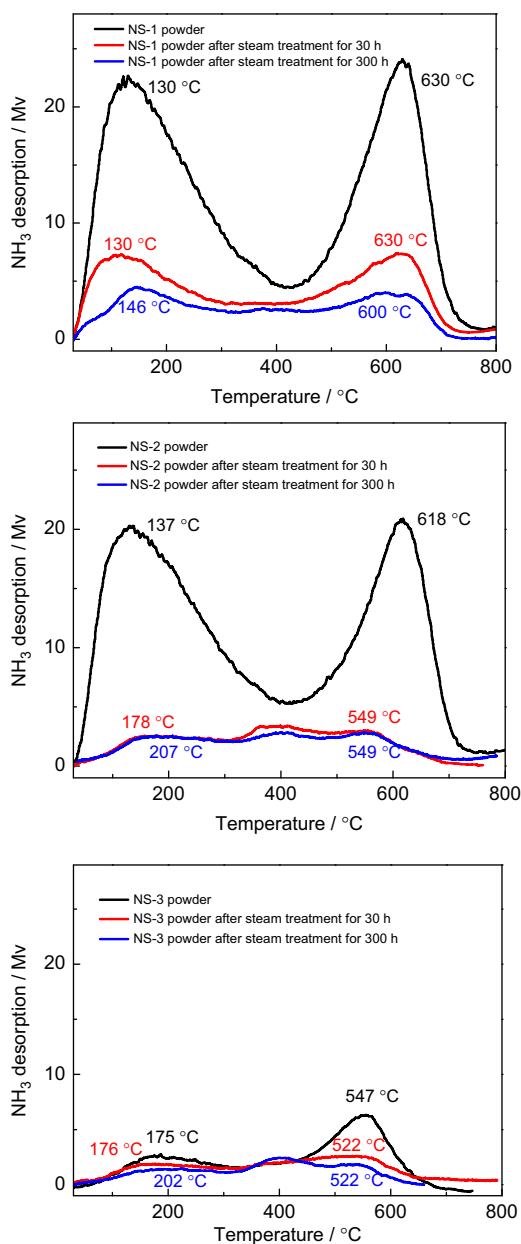
and NH_3-TPD records of the corresponding powders, before and after steam treatment, as displayed in Fig. 9,11 and 12, we can interpret the H_2 and CO_2 permeances variation of NS-1 and NS-2 membranes during the steam treatment as follows. The densification of the membrane should be responsible for the reduction of H_2 permeance for the initial 30 h, and the subsequently invulnerable membrane structure resulted in a steady H_2 permeance as steam exposure time prolonged. Meanwhile, if we pay attention to the decreasing rate of the CO_2 permeance, we can inferred that both densification process and acid sites presented in the membrane surface centers should be responsible for the dramatically decreased CO_2 permeance, as NS-1 and NS-2 membranes being in contact with hot steam. As for NS-1 membrane, CO_2 permeance decreased dramatically, giving the fact that the CO_2 permeance was below the detection limit after the membrane was steam-treated for only 50 h. While this decreasing rate was much more delayed for NS-2 membrane, which displayed a CO_2 permeance that was below the detection limit only after 100 h. If the acid sites presented in the membrane do not affect the CO_2 transportation, NS-2 membrane should exhibit higher decreasing rate of CO_2 permeance in comparison with that of NS-1 membrane. The result lines up with the fact that the Lewis acidity of Nb_2O_5-SiO_2 powders decreased as the Nb adding amount increased, as reported by Burke and Ko [61]. The Py-IR spectrum of NS-2 powders after exposed to 1000 kPa steam for 300 h shown in Fig. 4 displayed absorption signals reflecting Lewis acidity, which in part corroborated the generated acid sites in the membrane surface centers. As for NS-3 membrane, CO_2 permeance can always be detected, even if the steam treatment time was as long as 300 h. This phenomenon was totally different as that found for NS-1 and NS-2 membranes. It seemed that both densification and acidity of membrane surfaces have little effect on CO_2 transportation through NS-3 membrane. The calculated effective surfaces of NS powders before and after steam exposure by using CO_2 adsorption data as shown in Fig. 11, confirmed aforementioned discussion, which can be found in Table S2. The XPS results of NS-2 powders before and after steam treatment shown in Fig. 13 verified the stability of membrane micro-structures, as evidenced by no visible shift of O1s peaks took place. Meanwhile, the XPS spectra (Table S3) indicated that the membrane structures were always composed of Nb–O–Nb, Nb–O–Si bridges. XRD patterns and FT-IR spectra of the NS-1∼NS-4 powders after steam treatment was illustrated in Figs. S3 and S4. In comparison with the corresponding NS powders before steam treatment, all NS powders showed amorphous phase after exposure to 1000 kPa steam for as long as 300 h. Additionally, the NS powders displayed almost the same absorption bands as that found for untreated powders, indicating the integrity of the membrane structures retained although undergone harsh steam treatment.

Fig. 12. NH_3-TPD spectra of the calcined NS powders before and after steam treatment.

4. Conclusions

Niobium-BTESE derived hybrid silica membranes exhibiting sufficient high H_2/CO_2 separation performances and excellent hydrothermal stability, were fabricated by using sol–gel method. The observed excellent H_2/CO_2 permselectivity is due to the incorporation of Nb into hybrid silica networks and, hence, creates new Lewis acid sites. Effect of the niobium addition amount on H_2/CO_2 separation properties of NS membranes, especially on hydrothermal stability, was investigated in detail.

With respect to the NS-1 and NS-2 membranes, both densified hybrid siliceous microporous networks and generated Lewis acid sites imparted very low CO_2 permeance ($\sim 4 \times 10^{-10}$ mol m^{-2} s^{-1} pa^{-1}) to membranes due to the incorporation of Nb into the sol–gel derived bridged polysilsesquioxanes structures. One the other hand, as the Nb
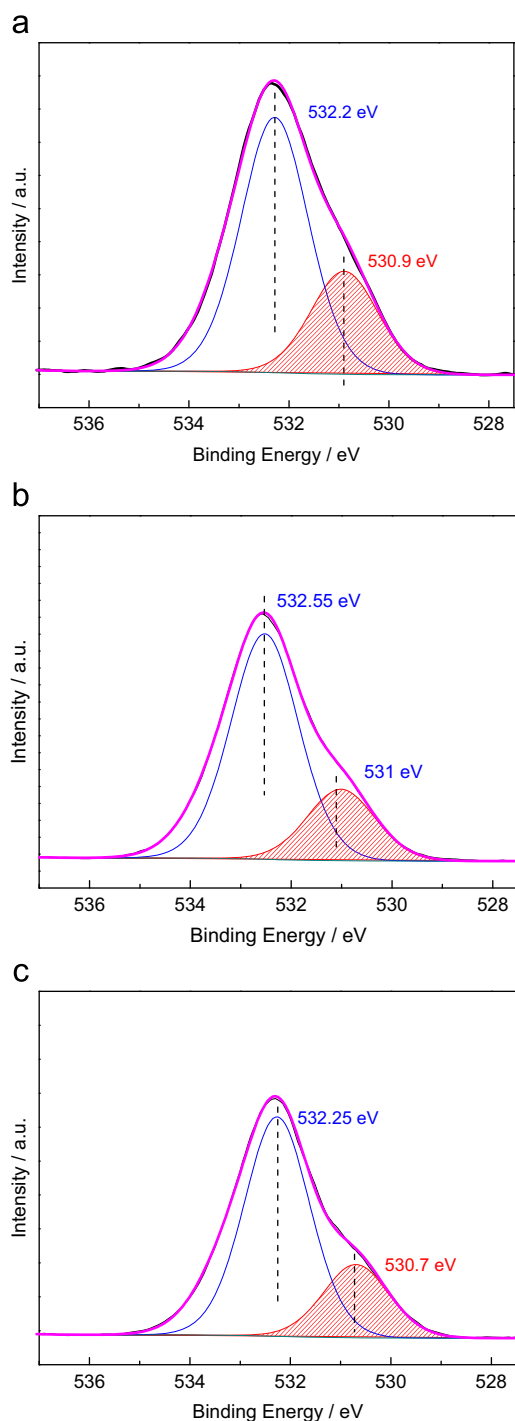
Fig. 13. XPS spectrum of the O 1s region for the calcined NS powders before and after hydrothermal treatment, which is fitted with a Gaussian distribution. (a) NS-2 powder. (b) NS-2 powder after hydrothermal treatment for 30 h. (c) NS-2 powder after hydrothermal treatment for 300 h.).

content was less than 50% (in mole), those membranes retained comparatively high H_2 permeance in the order of $\sim 6 \times 10^{-8}$ mol m^{-2} s^{-1} pa^{-1}, which allows the H_2/CO_2 permselectivity reached a value as high as 120. Dominant densification shall take effect when the Nb content was higher than 50%, which leads to both low H_2 permeance and H_2/CO_2 permselectivity of NS-3 and NS-4 membranes. The variation of amount and/or density of linkages, including Nb–O–Nb, Nb–O–Si and Si–O–Si bonds, which comprised Nb-hybrid silica membranes, should be responsible for the variation of membrane performances. Both NS-1 and NS-2 membranes showed

excellent stabilities in the presence of 150 kPa steam under 200 °C, as evidenced by the steady H_2 permeance ($\sim 2 \times 10^{-8}$ mol m^{-2} s^{-1} pa^{-1}) and exceptionally high H_2/CO_2 permselectivity (ca. 1500) during long-term stability test up to 300 h. The densification of the membrane in contact with the hot vapor should be responsible for the reduction of the H_2 permeance for the initial 30–100 h, and the subsequently invulnerable membrane structures resulted in a steady H_2 permeance as steam exposure time prolonged. The results indicated that Nb-hybrid silica membranes hold great promises for integration in pre-combustion CO_2 capture technologies.

Acknowledgments

Appendix A. Supporting information

Supplementary data associated with this article can be found in the online version at http://dx.doi.org/10.1016/j.memsci.2012.07.010.

References

[1] R. Bredesen, T.A. Peters, Membranes in energy systems with CO_2 capture, Membr. Energy Convers. 2 (2008) 217–244.
[2] B. Metz, O. Davidson, H. de Coninck, M. Loos, L. Meyer, IPCC Special Report on Carbon Dioxide Capture and Storage, Cambridge University Press, New York, 2005.
[3] H. Qi, J. Han, N.P. Xu, H.J.M. Bouwmeester, Hybrid organic–inorganic microporous membranes with high hydrothermal stability for the separation of carbon dioxide, ChemSusChem 3 (2010) 1375–1378.
[4] M.L. Mottern, K. Shqau, J.Y. Shi, H. Verweij, Thin supported inorganic membranes for energy-related gas and water purification, Int. J. Hydrogen Energy 32 (2007) 3713–3723.
[5] L.L. Zhang, I.S. Park, K. Shqau, W.S. WinstonHo, H. Verweij, Supported inorganic membranes: promises and challenges, JOM 61 (2009) 61–71.
[6] H. Verweij, Y.S. Lin, J.H. Dong, Microporous silica and zeolite membranes for hydrogen purification, MRS Bull. 31 (2006) 756–764.
[7] K. . Okamoto, H. Kita, K. Horii, K. Tanaka, Zeolite NaA membrane: preparation, single-gas permeation, and pervaporation and vapor permeation of water/organic liquid mixtures, Ind. Eng. Chem. Res. 40 (2001) 163–175.
[8] T. Tomita, K. Nakayama, H. Sakai, Gas separation characteristics of DDR type zeolite membrane, Microporous Mesoporous Mater. 68 (2004) 71–75.
[9] R. Krishna, J.M. van Baten, In silico screening of zeolite membranes for CO_2 capture, J. Membr. Sci. 360 (2010) 323–333.
[10] F.K. Katsaros, T.A. Steriotis, G.E. Romanos, M. Konstantakou, A.K. Stubos, N.K. Kanellopoulos, Preparation and characterisation of gas selective microporous carbon membranes, Microporous Mesoporous Mater. 99 (2007) 181–189.
[11] P.S. Tin, T.S. Chung, Y. Liu, R. Wang, Separation of CO_2/CH_4 through carbon molecular sieve membranes derived from P84 polyimide, Carbon 42 (2004) 3123–3131.
[12] S.S. Hosseini, T.S. Chung, Carbon membranes from blends of PBI and polyimides for N_2/CH_4 and CO_2/CH_4 separation and hydrogen purification, J. Membr. Sci. 328 (2009) 174–185.
[13] T. Kai, S. Kazama, Y. Fujioka, Development of cesium-incorporated carbon membranes for CO_2 separation under humid conditions, J. Membr. Sci. 342 (2009) 14–21.
[14] R.M. de Vos, H. Verweij, High-selectivity, high-flux silica membranes for gas separation, Science 279 (1998) 1710–1711.
[15] G. Xomeritakis, C.Y. Tsai, Y.B. Jiang, C.J. Brinker, Tubular ceramic-supported sol–gel silica-based membranes for flue gas carbon dioxide capture and sequestration, J. Membr. Sci. 341 (2009) 30–36.
[16] V. Boffa, J.E. ten Elshof, A.V. Petukhov, D.H.A. Blank, Microporous niobia-silica membrane with very low CO_2 permeability, ChemSusChem 1 (2008) 437–443.

[17] Y.F. Gu, P. Hacarlioglu, S.T. Oyama, Hydrothermally stable silica-alumina composite membranes for hydrogen separation, J. Membr. Sci. 310 (2008) 28–37.

[18] T. Tsuru, Nano/subnano-tuning of porous ceramic membranes for molecular separation, J. Sol–Gel Sci. Technol. 46 (2008) 349–361.

[19] S. Battersby, T. Tasaki, S. Smart, B. Ladewig, S.M. Liu, M.C. Duke, V. Rudolph, J.C. Diniz da Costa, Performance of cobalt silica membranes in gas mixture separation, J. Membr. Sci. 329 (2009) 91–98.

[20] M.W.J. Luiten, N.E. Benes, C. Huiskes, H. Kruidhof, A. Nijmeijer, Robust method for micro-porous silica membrane fabrication, J. Membr. Sci. 348 (2010) 1–5.

[21] R. Igi, T. Yoshika, Y.H. Ikuhara, Y. Iwamoto, T. Tsuru, Characterization of Co-doped silica for improved hydrothermal stability and application to hydrogen separation membranes at high temperatures, J. Am. Ceram. Sci. 91 (2008) 2975–2981.

[22] S. Gopalakrishnan, J.C. Diniz da Costa, Hydrogen gas mixture separation by CVD silica membrane, J. Membr. Sci. 323 (2008) 144–147.

[23] H.R. Lee, T. Shibata, M. Kanezashi, T. Mizumo, J. Ohshita, T. Tsuru, Pore-size-controlled silica membranes with disiloxane alkoxides for gas separation, J. Membr. Sci. 383 (2011) 152–158.

[24] Y.F. Gu, S.T. Oyama, High molecular permeance in a poreless ceramic membrane, Adv. Mater. 19 (2007) 1636–1640.

[25] V. Boffa, J.E. ten Elshof, R. Garcia, D.H.A. Blank, Microporous niobia-silica membranes: Influence of sol composition and structure on gas transport properties, Microporous Mesoporous Mater. 118 (2009) 202–209.

[26] M.C. Duke, J.C. Diniz da Costa, D.D. Do, P.G. Gray, G.Q. Lu, Hydrothermally robust molecular sieve silica for wet gas separation, Adv. Funct. Mater. 16 (2006) 1215–1220.

[27] V. Boffa, D.H.A. Blank, J.E. ten Elshof, Hydrothermal stability of microporous silica and niobia-silica membranes, J. Membr. Sci. 319 (2008) 256–263.

[28] S. Battersby, S. Smart, B. Ladewig, S.M. Liu, M.C. Duke, V. Rudolph, J.C. Diniz da Costa, Hydrothermal stability of cobalt silica membranes in a water gas shift membrane reactor, Sep. Purif. Technol. 66 (2009) 299–305.

[29] M. Kanezashi, M. Sano, T. Yoshioka, T. Tsuru, Extremely thin Pd-silica mixed-matrix membranes with nano-dispersion for improved hydrogen permeability, Chem. Commun. 46 (2010) 6171–6173.

[30] D. Uhlmann, S.M. Liu, B.P. Ladewig, J.C. Diniz da Costa, Cobalt-doped silica membranes for gas separation, J. Membr. Sci. 326 (2009) 316–321.

[31] E.J. Kappert, A. Nijmeijer, N.E. Benes, Expeditious calcination of inorganic membranes by an instant temperature increment, Microporous Mesoporous Mater. 151 (2012) 211–215.

[32] B.A. McCool, W.J. DeSisto, Amion-functionalized silica membrances for ehanced carbon dioxide permeation, Adv. Funct. Mater. 15 (2005) 1635–1640.

[33] C.Y. Tsai, S.Y. Tam, Y.F. Lu, C.J. Brinker, Dual-layer asymmetric microporous silica membranes, J. Membr. Sci. 169 (2000) 255–268.

[34] T. Tsuru, R. Igi, M. Kanezashi, T. Yoshioka, S. Fujisaki, Y. Iwamoto, Permeation properties of hydrogen and water vapor through porous silica membranes at high temperatures, AIChE J. 57 (2011) 618–629.

[35] R. Kreiter, M.D.A. Rietkerk, B.C. Bonekamp, H.M. van Veen, V.G. Kessler, J.F. Vente, Sol–gel routes for microporous zirconia and titania membranes, J. Sol–Gel Sci. Technol. 48 (2008) 203–211.

[36] G.I. Spijksma, C. Huiskes, N.E. Benes, H. Kruidhof, D.H.A. Blank, V.G. Kessler, H.J.M. Bouwmeester, Microporous zirconia-titania composite membranes derived from diethanolamine-modified precursors, Adv. Mater. 18 (2006) 2165–2168.

[37] R.J.R. Uhlhorn, M.H.B.J. Huis In't Veld, K. Keizer, A.J. Burggraaf, High perms-electivities of microporous silica-modified γ-alumina membranes, J. Mater. Sci. Lett. 8 (1989) 1135–1138.

[38] H.L. Castricum, A. Sah, R. Kreiter, D.H.A. Blank, J.F. Vente, J.E. ten Elshof, Hybrid ceramic nanosieves: stabilizing nanopores with organic links, Chem. Commun. (2008) 1103–1105.

[39] T. Tsuru, H. Shintani, T. Yoshioka, M. Asaeda, A bimodal catalytic membrane having a hydrogen-permselective silica layer on a bimodal catalytic support: preparation and application to the steam reforming of methane, Appl. Catal., A: General 302 (2006) 78–85.

[40] M. Kanezashi, M. Asaeda, Hydrogen permeation characteristics and stability of Ni-doped silica membranes in steam at high temperature, J. Membr. Sci. 271 (2006) 86–93.

[41] T. Tsuru, T. Morita, H. Shintani, T. Yoshioka, M. Asaeda, Membrane reactor performance of steam reforming of methane using hydrogen-permselective catalytic SiO₂ membranes, J. Membr. Sci. 316 (2008) 53–62.

[42] K. Brands, D. Uhlmann, S. Smart, M. Bram, J.C. Diniz da Costa, Long-term flue gas exposure effects of silica membranes on porous steel substrate, J. Membr. Sci. 359 (2010) 110–114.

[43] Y.F. Gu, S.T. Oyama, Permeation properties and hydrothermal stability of silica-titania membranes supported on porous alumina substrates, J. Membr. Sci. 345 (2009) 267–275.

[44] G.P. Fotou, Y.S. Lin, S.E. Pratsinis, Hydrothermal stability of pure and modified microporous silica membranes, J. Mater. Sci. 30 (1995) 2803–2808.

[45] R.M. de Vos, W.F. Maier, H. Verweij, Hydrophobic silica membranes for gas separation, J. Membr. Sci. 158 (1999) 277–288.

[46] Q. Wei, F. Wang, Z.R. Nie, C.L. Song, W.Y. Lang, Q.Y. Li, Highly hydrothermally stable microporous silica membranes for hydrogen separation, J. Phys. Chem. B 112 (2008) 9354–9359.

[47] M. Kanezashi, K. Yada, T. Yoshioka, T. Tsuru, Design of silica networks for development of highly permeable hydrogen separation membranes with hydrothermal stability, J. Am. Chem. Soc. 131 (2009) 414–415.

[48] R. Kreiter, M.D.A. Rietkerk, H.L. Castricum, H.M. van Veen, J.E. ten Elshof, J.F. Vente, Evaluation of hybrid silica sols for stable microporous membranes using high-throughput screening, J. Sol–Gel Sci. Technol. 57 (2011) 245–252.

[49] M. Kanezashi, K. Yada, T. Yoshioka, T. Tsuru, Organic-inorganic hybrid silica membranes with controlled silica network size: Preparation and gas permeation characteristics, J. Membr. Sci. 348 (2010) 310–318.

[50] H.L. Castricum, G.G. Paradis, M.C. Mittelmeijer-Hazeleger, R. Kreiter, J.F. Vente, J.E. ten Elshof, Tailoring the separation behavior of hybrid organosilica membranes by adjusting the structure of the organic bridging group, Adv. Funct. Mater. 21 (2011) 2319–2329.

[51] H.L. Castricum, A. Sah, R. Kreiter, D.H.A. Blank, J.F. Vente, J.E. ten Elshof, Hydrothermally stable molecular separation membranes from organically linked silica, J. Mater. Chem. 18 (2008) 2150–2158.

[52] H. Qi, J. Han, N.P. Xu, Effect of calcination temperature on carbon dioxide separation properties of a novel microporous hybrid silica membrane, J. Membr. Sci. 382 (2011) 231–237.

[53] I. Nowak, M. Ziolek, Niobium compounds: preparation, characterization, and application in heterogeneous catalysis, Chem. Rev. 99 (1999) 3603–3624.

[54] T. Okuhara, Water-tolerant solid acid catalysts, Chem. Rev. 102 (2002) 3641–3666.

[55] A. Aronne, M. Turco, G. Bagnasco, G. Ramis, E. Santacesaria, M.D. Serio, E. Marenna, M. Bevilacqua, C. Cammarano, E. Fanelli, Gel derived niobium-silicon mixed oxides: Characterization and catalytic activity for cyclooctene epoxidation, Appl. Catal. A: General 347 (2008) 179–185.

[56] A. Aronne, M. Turco, G. Bagnasco, P. Pernice, M.D. Serio, N.J. Clayden, E. Marenna, E. Fanelli, Synthesis of high surface area phosphosilicate glasses by a modified sol–gel method, Chem. Mater. 17 (2005) 2081–2090.

[57] M. Khatamian, A.A. Khandar, M. Haghighi, M. Ghadiri, M. Darbandi, Synthesis, characterization and acidic properties of nanopowder ZSM-5 type ferrisili-cates in the Na⁺/K⁺ alkali system, Powder Technol. 203 (2010) 503–509.

[58] C. Costa, I.P. Dzikh, J.M. Lopes, F. Lemos, F.R. Ribeiro, Activity-acidity relation-ship in zeolite ZSM-5. Application of Brönsted-type equations, J. Mol. Catal. A: Chem. 154 (2000) 193–201.

[59] R.S. Araújo, D.A.S. Maia, D.C.S. Azevedo, C.L. Cavalcante Jr, E. Rodríguez-Castellón, A. Jimenez-Lopez, Assessment of surface acidity in mesoporous materials containing aluminum and titanium, Appl. Surf. Sci. 255 (2009) 6205–6209.

[60] D. Prasetyoko, Z. Ramli, S. Endud, H. Nur, Preparation and characterization of bifunctional oxidative and acidic catalysts Nb₂O₅/TS-1 for synthesis of diols, Mater. Chem. Phys. 93 (2005) 443–449.

[61] P.A. Burke, E.I. Ko, Acidic properties of oxides containing niobia on silica and niobia in silica, J. Catal. 129 (1991) 38–46.

[62] M.S.P. Francisco, Y. Gushikem, Synthesis and characterization of SiO₂–Nb₂O₅ systems prepared by the sol–gel method: structural stability studies, J. Mater. Chem. 12 (2002) 2552–2558.

[63] E.B. Pereira, M.M. Pereira, Y.L. Lam, C.A.C. Perez, M. Schmal, Synthesis and characterization of niobium oxide layers on silica and the interaction with nickel, Appl. Catal. A: General 197 (2000) 99–106.

[64] R.Q. Long, R.T. Yang, Selective catalytic oxidation of ammonia to nitrogen over Fe₂O₃-TiO₂ prepared with a sol–gel method, J. Catal. 207 (2002) 158–165.

[65] R.V.R.A. Rios, J. Silvestre-Albero, A. Sepúlveda-Escribano, M. Molina-Sabio, F. Rodríguez-Reinoso, Kinetic restrictions in the characterization of narrow microporosity in carbon materials, J. Phys. Chem. C 111 (2007) 3803–3805.

[66] V.S. Braga, J.A. Dias, S.C.L. Dias, J.L. de Macedo, Catalyst materials based on Nb₂O₅ supported on SiO₂–Al₂O₃: Preparation and structural characterization, Chem. Mater. 17 (2005) 690–695.

[67] M. Barczak, A. Dabrowski, J. Ryczkowski, S. Pasieczna-Patkowska, FT-IR/PAS studies of ethylene-bridged polysilses-quioxanes functionalized with differ-ent groups, Eur. Phys. J. Spectrosc. Top. 154 (2008) 301–304.

[68] S.K. Medda, D. Kundu, G. De, Inorganic–organic hybrid coatings on poly-carbonate. Spectroscopic studies on the simultaneous polymerizations of methacrylate and silica networks, J. Non-Cryst. Solids 318 (2003) 149–156.

[69] L. Zhang, J.Y. Ying, Synthesis and characterization of mesoporous niobium-doped silica molecular sieves, AIChE J. 43 (1997) 2973–2801.

[70] Y. Kawano, S. Denofre, Y. Gushikem, Raman and infrared spectra of silica gel and niobium(V) oxide grafted on silica gel surface and their dependence on pretreatment temperatures, Vib. Spectrosc. 7 (1994) 293–302.

[71] L.J. Burcham, J. Datka, I.E. Wachs, In situ vibrational spectroscopy studies of supported niobium oxide catalysts, J. Phys. Chem. B 103 (1999) 6015–6024.

[72] J. Mendez-Vivar, P. Bosch, V.H. Lara, FTIR spectroscopy and x-ray diffraction characterization of Nb doped sol–gel silica, J. Sol–Gel Sci. Technol. 6 (1996) 257–262.

[73] L. Dragone, P. Moggi, G. Predieri, R. Zanoni, Niobia and silica–niobia catalysts from sol–gel synthesis: an X-ray photoelectron spectroscopic characteriza-tion, Appl. Surf. Sci. 187 (2002) 82–88.

[74] S. Damyanova, L. Dimitrov, L. Petrov, P. Grange, Effect of niobium on the surface properties of Nb₂O₅–SiO₂-supported Mo catalysts, Appl. Surf. Sci. 214 (2003) 68–74.

[75] W.F. Du, K. Kuraoka, T. Akai, T. Yazawa, Study of Al2O3 effect on structural change and phase separation in Na₂O-B₂O₃-SiO₂ glass by NMR, J. Mater. Sci. 35 (2000) 4865–4871.

[76] K.O. Drake, D. Carta, L.J. Skipper, F.E. Sowrey, R.J. Newport, M.E. Smith, A multinuclear solid state NMR study of the sol–gel formation of amorphous Nb₂O₅-SiO₂ materials, Solid State Nucl. Magn. Reson. 27 (2005) 28–36.

[77] R.M. de Vos, H. Verweij, Improved performance of silica membranes for gas separation, J. Membr. Sci. 143 (1998) 37–51.